Available online at www.sciencedirect.com
SCIENCE DIRECT®
Journal of Sound and Vibration 278 (2004) 21–38
JOURNAL OF SOUND AND VIBRATION
www.elsevier.com/locate/jsvi

Frequency-domain generalized total least-squares identification for modal analysis

P. Verboven*, P. Guillaume, B. Cauberghe, E. Parloo, S. Vanlanduit

Department of Mechanical Engineering, Vrije Universiteit Brussel, Acoustics and Vibration Research Group, Pleinlaan 2, B-1050 Brussels, Belgium

Received 25 June 2003; accepted 25 September 2003

Abstract

This contribution focuses on the area of modal analysis and studies the applicability of total least-squares (TLS) algorithms for the estimation of modal parameters in the frequency-domain from input–output Fourier data. These algorithms can be preferable to classical frequency response function based curve-fitting methods. This is certainly the case when periodic excitation is applied and an errors-in-variables noise model can be determined. The proposed generalized total least-squares (GTLS) algorithm provides an accurate modal parameter estimation by the integration of this noise model in the parametric identification process. Modal-based design and comfort improvement, damage assessment and structural health monitoring, and finite element model updating are important applications that strongly rely on a high accuracy of the modal model. In this paper it is shown how frequency-domain TLS and GTLS estimators can be numerically optimized to handle large amounts of modal data. In order to use an errors-in-variables noise model, a linear approximation is necessary in order to obtain a fast implementation of the GTLS algorithm. The validity of this approximation is a function of the signal-to-noise ratio of the input Fourier data and is evaluated by means of Monte Carlo simulations and experimental data.

1. Introduction

Modal parameter estimation has become a common technique used by engineers to analyze complex mechanical and civil structures such as cars, aircraft, industrial machinery, bridges, buildings, etc. The representation of the dynamical behaviour of such structures by means of the

*Corresponding author. Tel.: +32-2-629-2807; fax: +32-2-629-2865.
E-mail address: peter.verboven@vub.ac.be (P. Verboven).
URL: http://www.avrg.vub.ac.be.

0022-460X/$ - see front matter © 2003 Elsevier Ltd. All rights reserved.
doi:10.1016/j.jsv.2003.09.058

modal parameters (i.e., damped resonance frequencies, damping ratio and mode shapes) allows a better physical interpretation and a way to get condensed experimental data suitable for a variety of mechanical design purposes such as finite element model correlation, structural redesign as well as for structural damage assessment, monitoring and control applications.

The use of total least-squares (TLS) techniques for frequency-domain identification has already been extensively discussed in several publications (both for single input–single output (SISO) and multiple input–multiple output (MIMO) models) [1,2]. However, modal analysis has its typical characteristics such as extensive data sets (e.g., systems with 3 inputs and 500 outputs), high modal density with closely spaced modes, high dynamical range, and sometimes, depending on the application, medium to low signal-to-noise ratios. Another important feature of modal analysis identification is the use of so-called stabilization charts, useful to separate the physical modes from the mathematical ones. To construct these charts, pole estimates for different model orders are required. Consequently, TLS algorithms required some important adaptations to become applicable for modal analysis.

The common approach for experimental modal identification starts from frequency response functions (FRF), which are derived using a non-parametric FRF estimator such as H_1 or H_v. Next, the modal parameters are estimated using curve fitting schemes, such as, e.g., least-squares complex exponential (LSCE) [3], eigensystem realization (ERA) [4] or rational fractional polynomial (RFP) algorithms [5,6]. One of the most popular identification schemes used in the industry consists of a 2-step approach. First, based on the inverse FFT of this FRF data, the poles and modal participation factors (cf. Section 2.1) are estimated with the time-domain polyreference LSCE estimator for different model orders and poles are selected from a stabilization chart. In the second step, the poles are fixed in the modal model and the mode shapes are estimated by means of a Least-Squares frequency-domain (LSFD) solver.

However, as is well known, FRF-based identification can have serious drawbacks. First of all, FRF data is obtained using an non-parametric FRF estimator, such as the H_1, H_2 or H_v estimator [3]. Restrictive assumptions about the noise model make these FRF estimators inconsistent. FRF-based errors-in-variables modelling is possible when using the H_{iv} for arbitrary excitation [7] or H_{ev} in case of periodic excitation [8]. Furthermore, it is not meaningful to use these average-based FRF estimators when only short data sequences are available, since a minimal frequency resolution is required for accurate system identification. This is often the case for flight flutter testing and structural health monitoring practices (e.g., rotating machinery) due to cost, safety, and time-invariance reasons.

In this contribution the FRF-based TLS approach is extended to errors-in-variables modelling based on input/output Fourier modal data. In case of the generalized TLS (GTLS), the measurement noise can be incorporated in the estimation process, which improves the accuracy of the parameter estimates. A similar approach that was used for numerical optimization of the FRF-based TLS algorithms [7,9] is applied (cf. Section 3). Nevertheless, some important differences compared to these FRF-based algorithms can be noticed. In the case of the input–output GTLS approach, a fast implementation is not straightforward once the input noise sources are also taken into account. In Section 3 it is shown how this can be overcome using a linear approximation in the problem formulation. A validation of the TLS and GTLS algorithms is done by means of Monte Carlo simulations (Section 4), and experimental data from an aircraft slat track (Section 5).

2. Frequency-domain identification—MIMO systems

2.1. Parametric model

In this contribution, the frequency response function between output o and input i (for $o = 1, 2, \ldots, N_o$ and $i = 1, 2, \ldots, N_i$) is modelled using a common denominator transfer function model [10]

$$\hat{H}_{oi}(\omega_k, \theta) = \frac{n_{oi}(\omega_k, \theta)}{d(\omega_k, \theta)}, \tag{1}$$

with $n_{oi}(\omega_k, \theta) = \sum_{j=0}^{n} \Omega_j(\omega_k) b_{oij}$ the numerator polynomial and $d(\omega_k, \theta) = \sum_{j=0}^{n} \Omega_j(\omega_k) a_j$ the common-denominator polynomial. Using a discrete-time domain model, the polynomial basis functions are given by $\Omega_j(\omega_k) = \mathrm{e}^{-\mathrm{i}\omega_k T_s j}$ with T_s the sampling period, $k = 1, \ldots, N_f$ (N_f the number of spectral lines) and $j = 1, \ldots, n$ (n order of the polynomials). The polynomial coefficients a_j and b_{oij} are the (unknown) parameters θ to be estimated.

The goal is to determine the structural dynamics by means of the modal parameters, i.e., the modal frequencies, damping ratios and modal residues, of a pole-residue parameterization

$$\mathbf{G}(s) = \sum_{r=1}^{N_m} \frac{\mathbf{R}_r}{(s - p_r)} + \sum_{r=1}^{N_m} \frac{\mathbf{R}_r^*}{(s - p_r^*)}, \tag{2}$$

with p_r and $\mathbf{R}_r$, respectively, the poles and $(N_o \times N_i)$ residue matrices as model parameters corresponding to the rth mode of the structure ($N_m = n - 1$, the number of modes).

The modal parameters have to be derived from the estimates of the polynomial coefficients θ of the common-denominator model (1), which is done as follows

- *Poles*: the poles p_r $(r = 1, \ldots, N_m)$ are found as the roots of the common denominator polynomial $d(\omega, \theta)$ with coefficients θ_d. From the poles the modal frequency f_{d_r} and damping ratio ζ_r are readily obtained as

$$f_{\mathrm{d}_r} = \frac{\mathrm{Im}(p_r)}{2\pi} \quad \text{and} \quad \zeta_r = -\frac{\mathrm{Re}(p_r)}{|p_r|}. \tag{3}$$

- *Residues*: the residue matrices $\mathbf{R}_r$ $(N_o \times N_i)$ can be calculated from the coefficients θ as follows

$$R_{oir} = \lim_{\Omega \to p_r} \hat{H}_{oi}(\Omega, \theta)(\Omega - p_r). \tag{4}$$

If a discrete-time pole-residue model (Z-domain) is used, the poles p_r and residues $\mathbf{R}_r$ have to be transformed to the Laplace domain by means of the impulse-invariant transformation ($z = \mathrm{e}^{-sT_s}$), where the damped natural frequency and damping ratio are subsequently obtained from the poles as (3).

For modal analysis purposes, the residue matrices are further decomposed using the singular value decomposition algorithm as $\mathbf{R}_r = Q_r \boldsymbol{\Psi}_r \boldsymbol{\Psi}_r^{\mathrm{T}} = \boldsymbol{\Psi}_r \mathbf{L}_r^{\mathrm{T}}$ with $\boldsymbol{\Psi}_r$, $\mathbf{L}_r$, respectively, the mode shape and modal participation factor vector and Q_r the modal scale factor for mode r. Modal participation factors are a result of multiple reference (input) modal parameter estimation and define how each mode is excited from each of the input locations.

2.2. Errors-in-variables framework

In practice, the measured responses (velocities and/or accelerations) as well as forces are affected by errors, i.e., measurement noise and process noise (due to environmental influences which act as non-measured forces on the structure). Hence, as shown in Fig. 1, the measured I/O Fourier data $\mathbf{Z}(\omega_k) = [\mathbf{F}^{\mathrm{H}}, \mathbf{X}^{\mathrm{H}}]^{\mathrm{H}}$ can be represented using an *errors-in-variables* stochastic noise model

$$\left.\begin{array}{l} \mathbf{Z}(\omega_k) = \mathbf{Z}_0(\omega_k) + \mathbf{E}_Z(\omega_k) \\ [\mathbf{H}_0(\omega_k), -\mathbf{I}_{N_o}]\mathbf{Z}_0(\omega_k) = 0 \end{array}\right\}, \quad k = 1, \ldots, N_f \tag{5}$$

with $\mathbf{Z}_0(\omega_k) = [\mathbf{F}_0^{\mathrm{H}}, \mathbf{X}_0^{\mathrm{H}}]^{\mathrm{H}}$ the "*true*" input–output (I/O) Fourier data and $\mathbf{E}_Z(\omega_k) = [\mathbf{E}_F^{\mathrm{H}}, \mathbf{E}_X^{\mathrm{H}}]^{\mathrm{H}}$ some random perturbations, where the column vectors $\mathbf{Z}(\omega_k)$, $\mathbf{Z}_0(\omega_k)$, $\mathbf{E}_Z(\omega_k) \in \mathbb{C}^{N_i+N_o\times 1}$.

The errors $\mathbf{E}_Z(\omega_k)$ are assumed to be complex normally distributed with an a priori known covariance matrix

$$\mathbf{C}_{E_Z}(\omega_k) = \mathscr{E}\{\mathbf{E}_Z(\omega_k)\mathbf{E}_Z(\omega_k)^{\mathrm{H}}\} = \begin{pmatrix} \mathbf{C}_{E_F}(\omega_k) & \mathbf{C}_{E_F E_X}(\omega_k) \\ \mathbf{C}_{E_X E_F}(\omega_k) & \mathbf{C}_{E_X}(\omega_k) \end{pmatrix}, \tag{6}$$

where $\mathscr{E}$ the expected value operator. Taking, besides the noise variances, also the cross-correlations of the errors on the I/O Fourier data into account, can further decrease the

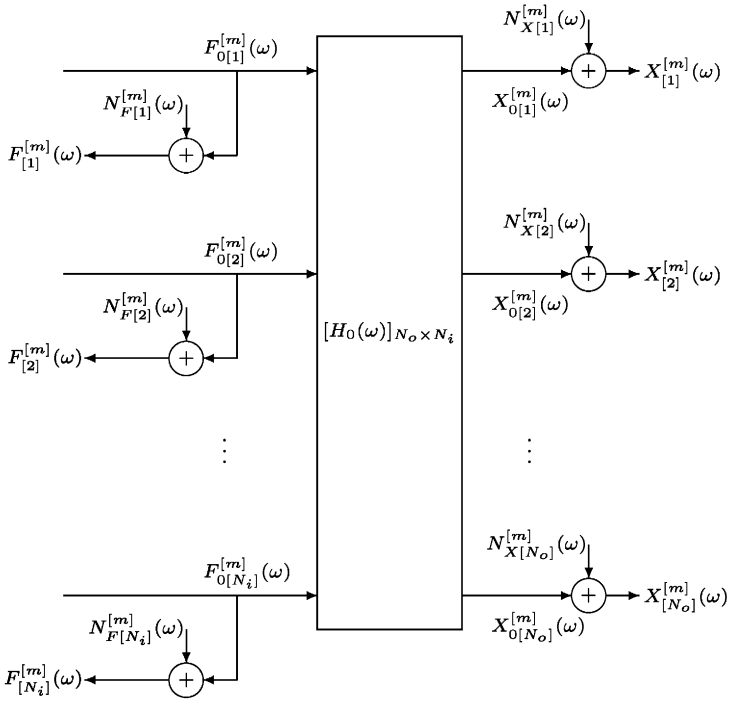

Fig. 1. Frequency-domain Errors-in-Variables noise model.

uncertainty of the estimates. However, in the case that the output correlations are considered, the time efficient implementation, presented in Section 3, cannot be applied. Moreover, since the covariance matrix $\mathbf{C}_{E_Z}(\omega_k)$ is usually obtained by means of measurements, obtaining a consistent estimate of the full output covariance matrix $\mathbf{C}_{E_X}(\omega_k)$ for a large number of responses (N_o) requires at each response location at least N_o measurements [11] and as a result only the output variances are used in practice. On the other hand, since the number of inputs is typically small ($N_i \leqslant 5$), input correlations as well as input–output correlations can be experimentally determined, resulting in $\mathbf{C}_{E_F}(\omega_k)$ and $\mathbf{C}_{E_X E_F}(\omega_k)$ being full matrices. In the next sections, correlations are only considered between the inputs, although a fast implementation is still possible when also the input–output correlations are used.

In practice, in the case that multiple periods are measured under periodic excitation, the elements of the noise covariance matrix can be simply computed using a sample (co-)variance approach. However, when arbitrary (e.g., random noise) excitation is used, an errors-in-variables noise model can still be obtained, although this requires an non-parametric instrumental variables approach of the Welch method [7].

2.3. Model equations

Using Eqs. (1) and (5) under the noise assumptions made in Section 2.2, the model equations are written for output o and spectral line k as (Levi's method)

$$\mathrm{W}_o(\omega_k)(\lfloor \mathbf{n}_o(\omega_k,\theta) \rfloor \{\mathbf{F}(\omega_k)\} - d(\omega_k,\theta)X_o(\omega_k)) \approx 0, \tag{7}$$

where $\{\mathbf{F}(\omega_k)\}$ represents the input Fourier vector and $\lfloor \mathbf{n}_o(\omega_k,\theta) \rfloor$ row o of the $(N_o \times N_i)$ numerator polynomial matrix. By introducing an adequate (frequency-dependent) weighting function $\mathrm{W}_o(\omega_k)$ in Eqs. (7), the quality of the parameter estimates can often be improved [2].

By estimating simultaneously initial conditions and the system model parameters, it is possible to deal with arbitrary signals in the frequency domain without any approximation and under the same assumptions as in the time-domain [12]. Using this approach, the proposed I/O GTLS estimator can be made robust against errors due to leakage effects, in a similar way as discussed in Ref. [13].

As Eqs. (7) are linear-in-the-parameters and in the Fourier data, they can be reformulated as $\mathbf{J}\boldsymbol{\theta} \approx 0$

$$\begin{bmatrix} \boldsymbol{\Gamma}_1 & 0 & 0 & \cdots & \boldsymbol{\Phi}_1 \\ 0 & \boldsymbol{\Gamma}_2 & 0 & \cdots & \boldsymbol{\Phi}_2 \\ \vdots & \vdots & \ddots & \vdots & \vdots \\ 0 & 0 & \cdots & \boldsymbol{\Gamma}_{N_o} & \boldsymbol{\Phi}_{N_o} \end{bmatrix} \begin{Bmatrix} \boldsymbol{\theta}_{n_1} \\ \boldsymbol{\theta}_{n_2} \\ \vdots \\ \boldsymbol{\theta}_{n_{N_o}} \\ \boldsymbol{\theta}_d \end{Bmatrix} \approx 0, \tag{8}$$

with $\mathbf{J}$ the Jacobian matrix now having $N_f N_o N_i$ rows and $(n+1)(N_o N_i + 1)$ columns. A similar formulation can be obtained for real coefficients for which the number of equations and coefficients is doubled. The entries of the submatrices $\boldsymbol{\Gamma}_o = [\boldsymbol{\Gamma}_{o1}, \ldots, \boldsymbol{\Gamma}_{oN_i}]$ $(N_f \times N_i.(n+1))$

and $\mathbf{\Phi}_o$ ($N_f \times (n+1)$) are given by

$$\mathbf{\Gamma}_{oi}(\omega_k) = \mathrm{W}_o(\omega_k)[\Omega_f^0, \Omega_f^1, \ldots, \Omega_f^n]F_i(\omega_k),$$
$$\mathbf{\Phi}_o(\omega_k) = -\mathrm{W}_o(\omega_k)[\Omega_f^0, \Omega_f^1, \ldots, \Omega_f^n]X_o(\omega_k), \tag{9}$$

while the parameter vector entries contain the (unknown) coefficients

$$\boldsymbol{\theta}_{n_o} = [b_{o10}, b_{o11}, \ldots, b_{oN_in}]^{\mathrm{T}}, \tag{10}$$

$$\boldsymbol{\theta}_d = [a_0, a_1, \ldots, a_n]^{\mathrm{T}}. \tag{11}$$

3. Fast weighted generalized TLS algorithm

This section, discusses a fast implementation for solving the model equations (8) in a weighted generalized total least-squares (WGTLS) approach.

Given that $N_f \gg n$, formulating the normal equations $\mathbf{J}^{\mathrm{H}}\mathbf{J}\boldsymbol{\theta} \approx 0$ results in a more compact formulation of the identification problem ($\mathbf{J}^{\mathrm{H}}\mathbf{J}$ having $(n+1)(N_o.N_i)$ rows and columns)

$$\begin{bmatrix} \mathbf{R}_1 & 0 & 0 & \cdots & \mathbf{S}_1 \\ 0 & \mathbf{R}_2 & 0 & \cdots & \mathbf{S}_2 \\ \vdots & \vdots & \ddots & \vdots & \vdots \\ 0 & 0 & \cdots & \mathbf{R}_{N_o} & \mathbf{S}_{N_o} \\ \mathbf{S}_1^{\mathrm{H}} & \mathbf{S}_2^{\mathrm{H}} & \cdots & \mathbf{S}_{N_o}^{\mathrm{H}} & \mathbf{T} \end{bmatrix} \begin{Bmatrix} \boldsymbol{\theta}_{n_1} \\ \boldsymbol{\theta}_{n_2} \\ \vdots \\ \boldsymbol{\theta}_{n_{N_o}} \\ \boldsymbol{\theta}_d \end{Bmatrix} \approx 0, \tag{12}$$

with matrices $\mathbf{R}_o$ having $(n+1).N_i$ rows and columns, $\mathbf{S}_o$ having $(n+1).N_i$ rows and $(n+1)$ columns, and $\mathbf{T} = \sum_o \mathbf{T}_o$ having $(n+1)$ rows and columns. The entries of the sub-matrices are given by

$$[\mathbf{R}_o^{i_1,i_2}]_{rs} = \sum_{f=1}^{N_f} |\mathrm{W}_o(\omega_f)|^2 F_{i_1}^*(\omega_f)F_{i_2}(\omega_f)\Omega_f^{r-1^{\mathrm{H}}}\Omega_f^{s-1},$$
$$[\mathbf{T}_o]_{rs} = \sum_{f=1}^{N_f} |\mathrm{W}_o(\omega_f)X_o(\omega_f)|^2 \Omega_f^{r-1^{\mathrm{H}}}\Omega_f^{s-1},$$
$$[\mathbf{S}_o^{i_1}]_{rs} = -\sum_{f=1}^{N_f} |\mathrm{W}_o(\omega_f)|^2 F_{i_1}^*(\omega_f)X_o(\omega_f)\Omega_f^{r-1^{\mathrm{H}}}\Omega_f^{s-1}. \tag{13}$$

A closer look at Eqs. (12) and (13) indicates that these matrices have a Toeplitz structure, which is beneficial for both computation time and memory usage. Moreover, if the frequencies are uniformly distributed, the fast Fourier transform (FFT) algorithm can be used to compute the entries of matrices $\mathbf{R}_o$, $\mathbf{S}_o$ and $\mathbf{T}_o$ [14,15]. The use of a discrete time-domain model leads to a well-conditioned Jacobian matrix, which justifies the explicit calculation of the normal equations. In the case of a continuous time-domain model, orthogonal polynomials (e.g., Forsythe or Chebyshev) can be used to improve the numerical conditioning [16].

A GTLS approach formulates Eq. (12) as an generalized eigenvalue problem (14),

$$\mathbf{J}^{\mathrm{H}}\mathbf{J}\theta = \lambda \mathbf{C}\boldsymbol{\theta} \tag{14}$$

with $\mathbf{C}$ being the covariance matrix containing a measure for the errors on the entries of the matrix $\mathbf{J}^{\mathrm{H}}\mathbf{J}$ as a result from measurement noise on the I/O Fourier data. Considering the errors-in-variables model with the noise assumptions made in Section 2.2, the generalized eigenvalue problem (14) is explicitly given as

$$\begin{bmatrix} \mathbf{R}_1 & 0 & \cdots & \mathbf{S}_1 \\ 0 & \mathbf{R}_2 & \cdots & \mathbf{S}_2 \\ \vdots & \vdots & \ddots & \vdots \\ \mathbf{S}_1^{\mathrm{H}} & \mathbf{S}_2^{\mathrm{H}} & \cdots & \mathbf{T} \end{bmatrix} \begin{Bmatrix} \boldsymbol{\theta}_{n_1} \\ \boldsymbol{\theta}_{n_2} \\ \vdots \\ \boldsymbol{\theta}_{n_{N_o}} \\ \boldsymbol{\theta}_d \end{Bmatrix} = \lambda \begin{bmatrix} \mathbf{C}_{R_1} & 0 & \cdots & \mathbf{C}_{S_1} \\ 0 & \mathbf{C}_{R_2} & \cdots & \mathbf{C}_{S_2} \\ \vdots & \vdots & \ddots & \vdots \\ \mathbf{C}_{S_1}^{\mathrm{H}} & \mathbf{C}_{S_2}^{\mathrm{H}} & \cdots & \mathbf{C}_T \end{bmatrix} \begin{Bmatrix} \boldsymbol{\theta}_{n_1} \\ \boldsymbol{\theta}_{n_2} \\ \vdots \\ \boldsymbol{\theta}_{n_{N_o}} \\ \boldsymbol{\theta}_d \end{Bmatrix}, \tag{15}$$

where $\mathbf{T} = \sum_{o=1}^{N_o} \mathbf{T}_o$ and $\mathbf{C}_T = \sum_{o=1}^{N_o} \mathbf{C}_{T_o}$. Given the Jacobian entries (9), the entries of the covariance matrix $\mathbf{C}$ are computed as $(i_1, i_2 = 1, \ldots, N_i)$

$$[\mathbf{C}_{R_o^{i_1 i_2}}]_{rs} = \mathscr{E}\{\delta\Gamma_{oi_1}^{\mathrm{H}} \delta\Gamma_{oi_2}\}_{rs} = \sum_{f=1}^{N_f} |\mathrm{W}_o(\omega_f)|^2 \,\mathrm{covar}(F_{i_2}(\omega_f), F_{i_1}(\omega_f)) \Omega_f^{r-1^{\mathrm{H}}} \Omega_f^{s-1},$$

$$[\mathbf{C}_{S_o^{i_1}}]_{rs} = -\mathscr{E}\{\delta\Gamma_{oi_1}^{\mathrm{H}} \delta\Phi_o\}_{rs} = -\sum_{f=1}^{N_f} |\mathrm{W}_k(\omega_f)|^2 \,\mathrm{covar}(X_o(\omega_f), F_{i1}(\omega_f)) \Omega_f^{r-1^{\mathrm{H}}} \Omega_f^{s-1},$$

$$[\mathbf{C}_{T_o}]_{rs} = \mathscr{E}\{\delta\Phi_o^{\mathrm{H}} \delta\Phi_o\}_{rs} = \sum_{f=1}^{N_f} |\mathrm{W}_k(\omega_f)|^2 \,\mathrm{var}(X_o(\omega_f)) \Omega_f^{r-1^{\mathrm{H}}} \Omega_f^{s-1}, \tag{16}$$

where $\mathrm{var}(X_o(\omega_f))$ are the diagonal elements of the (diagonal) output noise covariance matrix $\mathbf{C}_{E_Z}$ and $\mathrm{covar}(F_{i_2}(\omega_f), F_{i_1}(\omega_f))$ and $\mathrm{covar}(X_o(\omega_f), F_{i1}(\omega_f))$, respectively, the elements of the input noise $\mathbf{C}_{E_F}(\omega_f)$ and Input/Output noise covariance matrices $\mathbf{C}_{E_F E_X}(\omega_f)$ (cf. Eq. (6)). When a discrete-time model in the Z-domain is used with uniformly distributed frequencies, entries (16) can again be computed in a time-efficient manner by means of the FFT algorithm with the matrices $\mathbf{C}_{R_o}$, $\mathbf{C}_{S_k}$ and $\mathbf{C}_{T_k}$ having a Toeplitz structure.

The computation time can be further significantly reduced by eliminating the numerator coefficients $\boldsymbol{\theta}_{n_o}$, since only the denominator coefficients $\boldsymbol{\theta}_d$ are required to compute the system poles. In the case of I/O Fourier data, elimination of the numerator coefficients $\boldsymbol{\theta}_{n_o}$ in (14) yields

$$\boldsymbol{\theta}_{n_o} = [\mathbf{I} - \lambda \mathbf{R}_o^{-1} \mathbf{C}_{R_o}]^{-1} [\lambda \mathbf{R}_o^{-1} \mathbf{C}_{S_o} - \mathbf{R}_o^{-1} \mathbf{S}_o] \boldsymbol{\theta}_d, \tag{17}$$

from which it can be seen that an additional term in λ (with λ unknown) appears in the case that also the input noise sources are taken into account (i.e., $\mathbf{C}_{R_o} \neq 0$ and $\mathbf{C}_{S_o} \neq 0$).

It is noticed that for FRF-based GTLS identification such an additional term in λ does not occur since errors are only present on the FRF data, only present in the last $(n+1)$ columns/rows of the normal equations [17].

Consequently, a straightforward formulation of a compact generalized eigenvalue problem in the denominator coefficients θ_d is not possible by eliminating θ_{n_o} from the last n equations

of (14), i.e.,

$$\sum_{o=1}^{N_o} \mathbf{S}_o^{\mathrm{H}} \boldsymbol{\theta}_{n_o} + \mathbf{T}\boldsymbol{\theta}_d = \lambda \mathbf{C}_T \boldsymbol{\theta}_d \tag{18}$$

and as a result, the exact solution of the GTLS identification problem (14) is only given by solving (14). However, the computational load for solving this eigenvalue problem, in the case of typical modal analysis applications (i.e., $N_o = 500$, $N_i = 3$, $n = 50$), is not acceptable in practice.

One obvious way to benefit from the elimination approach is by considering only errors on the measured output sequences, with all matrices $\mathbf{C}_{R_o}$ and $\mathbf{C}_{S_o}$ equal to zero in Eqs. (15) and (17) resulting after eliminating the numerator coefficients in the following generalized eigenvalue problem in $\boldsymbol{\theta}_d$

$$\left[T - \sum_{o=1}^{N_o} \mathbf{S}_o^{\mathrm{H}} \mathbf{R}_o^{-1} \mathbf{S}_o \right] \boldsymbol{\theta}_d = \lambda \mathbf{C}_T \boldsymbol{\theta}_d. \tag{19}$$

Once the $\boldsymbol{\theta}_d$ coefficients are known, Eq. (17) (with $\mathbf{C}_{R_o} = 0$ and $\mathbf{C}_{S_o} = 0$) can be used to derive all numerator coefficients. However, ignoring the input noise sources has the important disadvantage of loosing the EV noise-model characteristics together with the consistency properties of the GTLS approach, which in practice implies less accuracy of the modal parameters.

Therefore, another option was considered in order to combine the time-efficient elimination process with the advantages of EV (GTLS) identification. Using a Taylor expansion, the inverse matrix $[\mathbf{I} - \lambda \mathbf{R}_o^{-1} \mathbf{C}_{\mathbf{R}_o}]^{-1}$ in Eq. (17) can be approximated as

$$[\mathbf{I} - \lambda \mathbf{R}_o^{-1} \mathbf{C}_{R_o}]^{-1} \cong \mathbf{I} + \lambda \mathbf{R}_o^{-1} \mathbf{C}_{R_o} + (\lambda \mathbf{R}_o^{-1} \mathbf{C}_{R_o})^2 + \cdots. \tag{20}$$

Introducing this approximation for the first order in Eq. (17) and substitution in Eq. (18) results in, after retaining the first order terms in λ

$$\boldsymbol{\theta}_{n_o} \cong -\mathbf{R}_o^{-1} \mathbf{S}_o \boldsymbol{\theta}_d - \lambda \mathbf{R}_o^{-1} \mathbf{C}_{R_o} \mathbf{R}_o^{-1} \mathbf{S}_o \boldsymbol{\theta}_d + \lambda \mathbf{R}_o^{-1} \mathbf{C}_{S_o} \boldsymbol{\theta}_d, \tag{21}$$

which now again yields a compact generalized eigenvalue problem in $\boldsymbol{\theta}_d$

$$\begin{aligned} &\sum_{o=1}^{N_o} [\mathbf{T}_o - \mathbf{S}_o^{\mathrm{H}} \mathbf{R}_o^{-1} \mathbf{S}_o] \boldsymbol{\theta}_d \\ &\quad = \lambda \sum_{o=1}^{N_o} \left[\mathbf{C}_{T_o} + \mathbf{S}_o^{\mathrm{H}} \mathbf{R}_o^{-1} \mathbf{C}_{R_o} \mathbf{R}_o^{-1} \mathbf{S}_o - 2\,\mathrm{herm}\left(\sum_{o=1}^{N_o} \mathbf{S}_o^{\mathrm{H}} \mathbf{R}_o^{-1} \mathbf{C}_{S_o} \right) \right] \boldsymbol{\theta}_d. \end{aligned} \tag{22}$$

Compared to Eq. (19), two additional terms in λ appear after linearizing, containing the noise characteristics of the input and between the input and output Fourier data, i.e., $\mathbf{C}_{R_o}$ and $\mathbf{C}_{S_o}$.

Notice that the matrix in the right part of Eq. (22) is the covariance matrix of the compact normal matrix

$$\mathbf{D} = \left[\mathbf{T} - \sum_{o=1}^{N_o} \mathbf{S}_o^{\mathrm{H}} \mathbf{R}_o^{-1} \mathbf{S}_o \right]. \tag{23}$$

Indeed, the covariance matrix $\mathbf{C}_D = \mathscr{E}\{\delta\mathbf{D}\}$ where

$$\delta\mathbf{D} = \sum_{o=1}^{N_o} \delta\mathbf{T}_o - \sum_{o=1}^{N_o} (\delta\mathbf{S}_o^{\mathrm{H}}\mathbf{R}_o^{-1}\mathbf{S}_o - \mathbf{S}_o^{\mathrm{H}}\mathbf{R}_o^{-1}\delta\mathbf{R}_o\mathbf{R}_o^{-1}\mathbf{S}_o + \mathbf{S}_o^{\mathrm{H}}\mathbf{R}_o^{-1}\delta\mathbf{S}_o) \tag{24}$$

and hence taking the expected value results in

$$\mathbf{C}_D = \left[\sum_{o=1}^{N_o} \mathbf{C}_{T_o} + \sum_{o=1}^{N_o} \mathbf{S}_o^{\mathrm{H}}\mathbf{R}_o^{-1}\mathbf{C}_{R_o}\mathbf{R}_o^{-1}\mathbf{S}_o - 2\,\mathrm{herm}\left(\sum_{o=1}^{N_o} \mathbf{S}_o^{\mathrm{H}}\mathbf{R}_o^{-1}\mathbf{C}_{S_o} \right) \right] \tag{25}$$

since $\mathbf{C}_{T_o} = \mathscr{E}\{\delta\mathbf{T}_o\}$, $\mathbf{C}_{R_o} = \mathscr{E}\{\delta\mathbf{R}_o\}$ and $\mathbf{C}_{S_o} = \mathscr{E}\{\delta\mathbf{S}_o\}$.

Instead of solving Eq. (14) directly, this elimination approach results in an important reduction of the computation time since the generalized singular value decomposition (GSVD) algorithm is applied to much smaller matrices (dimensions reduced by N_o^2). From Eq. (20) it follows that the linear approximation will be valid in the case that $\mathrm{EIG}(\mathbf{R}_o^{-1}\mathbf{C}_{R_o}) \ll \lambda$, where $\mathbf{R}_o^{-1}\mathbf{C}_{R_o}$ is a measure for the signal-to-noise ratio (SNR) of the input Fourier data. In the next section the validity of this linear approximation is studied by means of Monte Carlo simulations.

4. Monte Carlo simulation results

A SISO system having 6 modes with poles and residues given in Table 1 was used to generate an I/O data set of 1200 equally distributed frequencies in the band of 0.6–7.9 Hz: i.e., $F_0(\omega_k) = 1$, $X_0(\omega_k) = H_0(\omega_k)$ $(k = 1, \ldots, 1200)$. Independent zero-mean Gaussian noise was added to both the input and output data. In order to evaluate the validity of approximation (20) in the generalized eigenvalue problem (22), the variance of the input noise was increased over 21 logarithmically distributed steps in the range of $[10^{-8}, 1]$ while the output noise level remained constant with a variance of 1E-6. For each I/O noise combination, 1000 disturbed data sets were generated and for each set the modal parameters of 20 modes (poles, residues) were estimated using the estimators summarized in Table 2. The frequency weighting function $\mathbf{W}_o(\omega_f)$ was equal to 1 and $\mathbf{C}_S = 0$ for all estimators. Over-modelling is applied in order to deal with model errors related to the use of a discrete-time frequency-domain model (Z-domain).

Table 1
Poles and residues of simulated (exact) SISO transfer function

Mode	Pole	Residue
1	$-1.5234E-3+0.7500E+1\mathrm{i}$	$3.9282E-8+2.5015E-3\mathrm{i}$
2	$-1.3441E-3+1.2167E+1\mathrm{i}$	$1.2874E-7+1.4997E-3\mathrm{i}$
3	$-0.7553E-3+2.2164E+1\mathrm{i}$	$-4.9174E-6+1.1966E-3\mathrm{i}$
4	$-1.2464E-3+2.3837E+1\mathrm{i}$	$1.0541E-5+1.3087E-3\mathrm{i}$
5	$-0.5506E-3+2.5336E+1\mathrm{i}$	$-7.9402E-7+1.7064E-3\mathrm{i}$
6	$-1.1167E-3+4.4167E+1\mathrm{i}$	$1.2672E-9+1.9000E-3\mathrm{i}$

Table 2
Different estimators studied during Monte Carlo simulations ($\mathbf{C}_S = 0$ for all considered cases)

Estimator	Abbreviation	Description
Total Least-Squares	TLS	Eq. (15) with $\mathbf{C} = \mathrm{diag}(1,1)$
Fast TLS	FTLS	Eq. (19) with $\mathbf{C}_T = 1$
Generalized TLS	GTLS	Eq. (15)
Fast GTLS with input noise assumed zero	FGTLSX	Eq. (19) with $\mathbf{C}_R = 0$
Fast GTLS	FGTLS	Eq. (22)

It should be noticed that, by using an iterative approach, a fast I/O implementation of the bootstrapped TLS (BTLS) can be derived from Eq. (22) by choosing $\mathrm{W}_o(\omega_k)$ equal to the maximum likelihood weight calculated in the parameters from the previous iteration step [13].

The accuracy of the different estimators can be compared with respect to their squared bias, total variance and mean squared error (MSE) [18] for both the estimated poles and residues. These quantities are related as follows

$$\begin{aligned} MSE(\hat{P}) &= = \mathscr{E}\{(\hat{P} - P_0)^{\mathrm{H}}(\hat{P} - P_0)\} \\ &= \mathscr{E}\{(\hat{P} - \mathscr{E}\{\hat{P}\})^{\mathrm{H}}(\hat{P} - \mathscr{E}\{\hat{P}\})\} + (\mathscr{E}\{\hat{P}\} - P_0)^{\mathrm{H}}(\mathscr{E}\{\hat{P}\} - P_0) \\ &= \text{total variance}(\hat{P}) + \text{squared bias}(\hat{P}) \end{aligned} \tag{26}$$

with $\hat{P}$ and P_0 the estimated and theoretical values of the poles (residues). The Monte Carlo simulation results can be compared for the different estimators as shown in Fig. 2. As can also be noted in Table 2, the abbreviations of the different estimators are specially chosen: **F** indicates the fast implementation by taking specific matrix structures and elimination approach into account, **G** indicates the generalized TLS where an errors-in-variables (input/output) noise model is considered and **X** indicates a special case where only the noise sources on the responses are included in the errors-in-variables noise model (input noise is assumed to be zero).

The important errors in case of both TLS estimators are due to the high bias errors, originating from the inconsistency properties of the TLS approach, since no noise covariance information is taken into account. Considering only output noise results in the FGTLSX, improving the accuracy as long as the input variance is small. However, once the effect of the input noise outweighs the output noise, the errors for the FGTLSX increase significantly. Since input noise is disregarded, the FGTLSX is still inconsistent, explaining the increase in bias and the agreement with the TLS results for high input noise variances. The gain in accuracy by taking input noise into account is clearly illustrated by comparing the FGTLSX and the GTLS where the MSE is up to 10dB smaller for the GTLS. The good agreement of the errors for the GTLS and FGTLS indicates the validity of approximation (20). Only for very high variances of the input noise (SNR around 0dB), the errors are slightly higher for the FGTLS. This result proves that no loss in accuracy is encountered when using the approximation (within practical noise levels), making the fast implementation of the fast algorithm of the (W)GTLS suitable for an accurate analysis of large modal data sets.

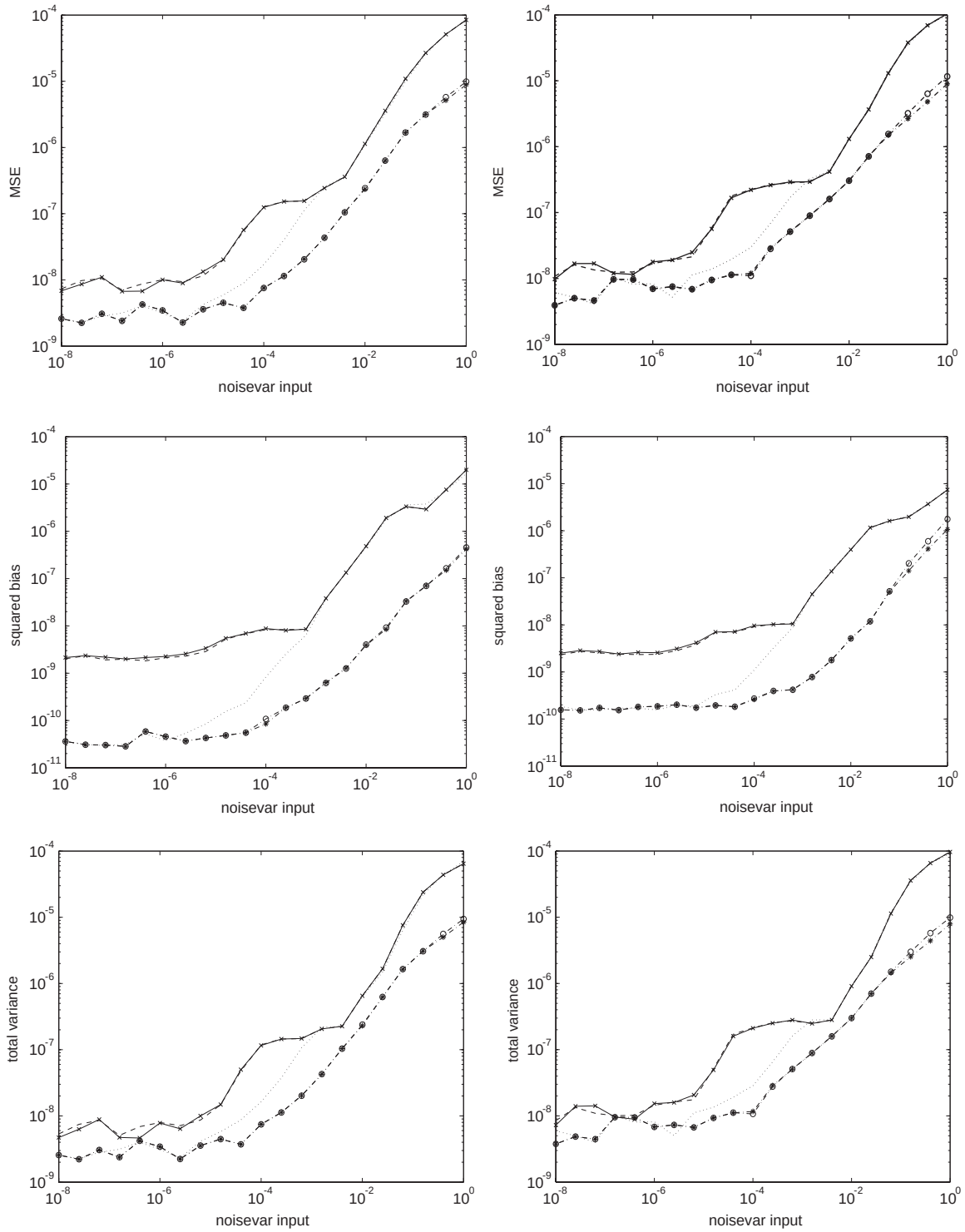

Fig. 2. Monte Carlo simulation results: mean squared error (MSE), squared bias and total variance for poles (left) and residues (right): GTLS (dashed–star), FGTLS (dashed–circle), FGTLSX (dots), TLS (dashed), FTLS (solid-cross).

5. Experimental results

The device under test is a slat track (cf. Fig. 3), which is a safety critical component in the wing of an aircraft, used to enlarge the wing surface during takeoff and landing when airspeed is reduced. The response to a single shaker input was measured at 352 points by means of a scanning laser Doppler vibrometer (SLDV) set-up (cf. Fig. 4). A broadband periodic (multisine) excitation was applied in a frequency band 0–4 kHz with 3200 spectral lines. Notice that this set-up is correctly characterized by the errors-in-variables noise model defined in Section 2.2, since every output is subsequently measured and hence the noise on the outputs is not correlated. In this case, the noise covariance matrix entries are obtained as the sample variances based on 5 periods (averages) for each output measurement (i.e., $C_{E_X} = 0$ and $C_{E_F E_X} = 0$).

Fig. 5 shows the ratio of a measured velocity and force and the transfer function model estimated by means of the FTLS and FGTLS for a model with 22 modes. The FGTLS has a better performance, explained by the use of noise covariance matrix information during the estimation process, making the FGTLS consistent and less sensitive to measurement noise. For the particular case of an SLDV set-up, measurement noise is mainly due to signal drop-outs and poor laser beam reflection when scanning points on edges of the ribs on slat track side (cf. Fig. 3).

For modal analysis, a stabilization chart is an important tool that is often used to assist the user in separating physical poles from mathematical ones (due to over-modelling) in order to select the

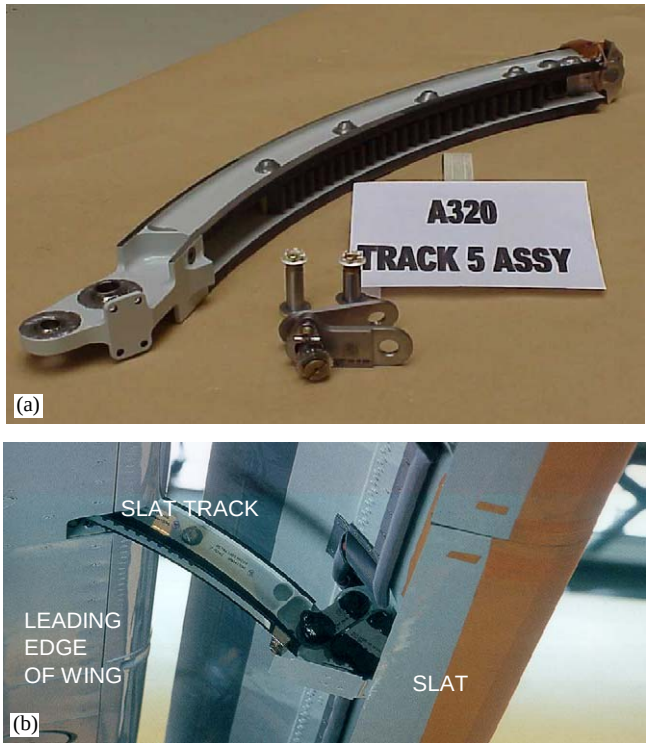

Fig. 3. A slat track (a) mounted in the wing of an Airbus320 aircraft (b).

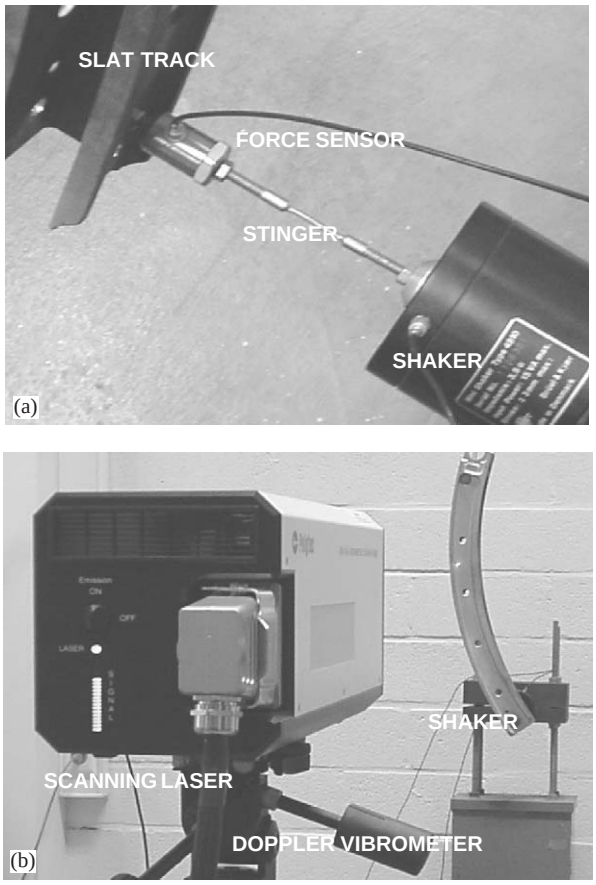

Fig. 4. Force (input) measurement with shaker, stinger and force sensor attached to the slat track (a). Velocity (output) measurement with scanning laser Doppler vibrometer (b).

structural modes. To construct this chart, the poles have to be estimated for increasing model orders as shown in Fig. 6, with (+) indicating stable poles and (×) unstable poles (i.e., positive real part), while the line is the averaged sum of all measurements. Since the model equations are formulated for a given maximum model order, the FGTLS problem can be re-solved for all smaller model orders by simply taking sub-matrices of the full matrices given in Eq. (22). By doing so, a set of FGTLS solutions is obtained for an increasing order of the denominator polynomial, while the order of the numerator polynomial is kept constant and equal to the maximum specified (polynomial) model order. This approach is very time efficient for constructing the stabilization chart. Comparing the charts for both estimators, it is clear that the use of a proper noise (EV) model results in an improved stabilization behaviour of the physical modes. In addition, the computational poles are estimated as unstable in the case of the FGTLS, improving the user friendliness of the chart, since in general, only the stable poles are plotted. Another important part of the modal model is the spatial information present in the estimated mode shapes. Fig. 7 shows the mode shape for the mode at 1234 Hz. Again the results obtained by the FGTLS are better

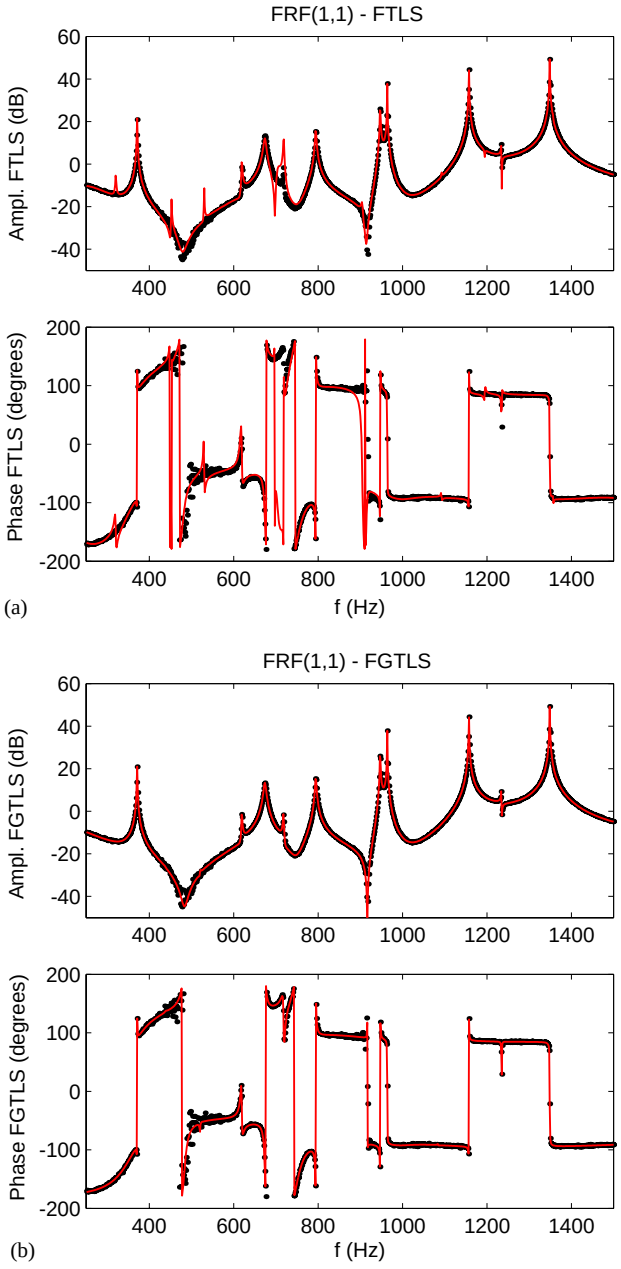

Fig. 5. Parametric results for the slat track using the FTLS (a), FGTLS (b) algorithm: amplitude and phase of the measurements (dotted line) and the estimated transfer function model (solid line).

since an accurate noise model is taken into account. The mode shape for the FTLS is clearly corrupted by the measurement noise.

Finally, the numerical efficiency is illustrated in Fig. 8 by comparing the GTLS and FGTLS algorithms in terms of (MATLAB) flops count for a varying number of outputs N_o (with $n = 20$,

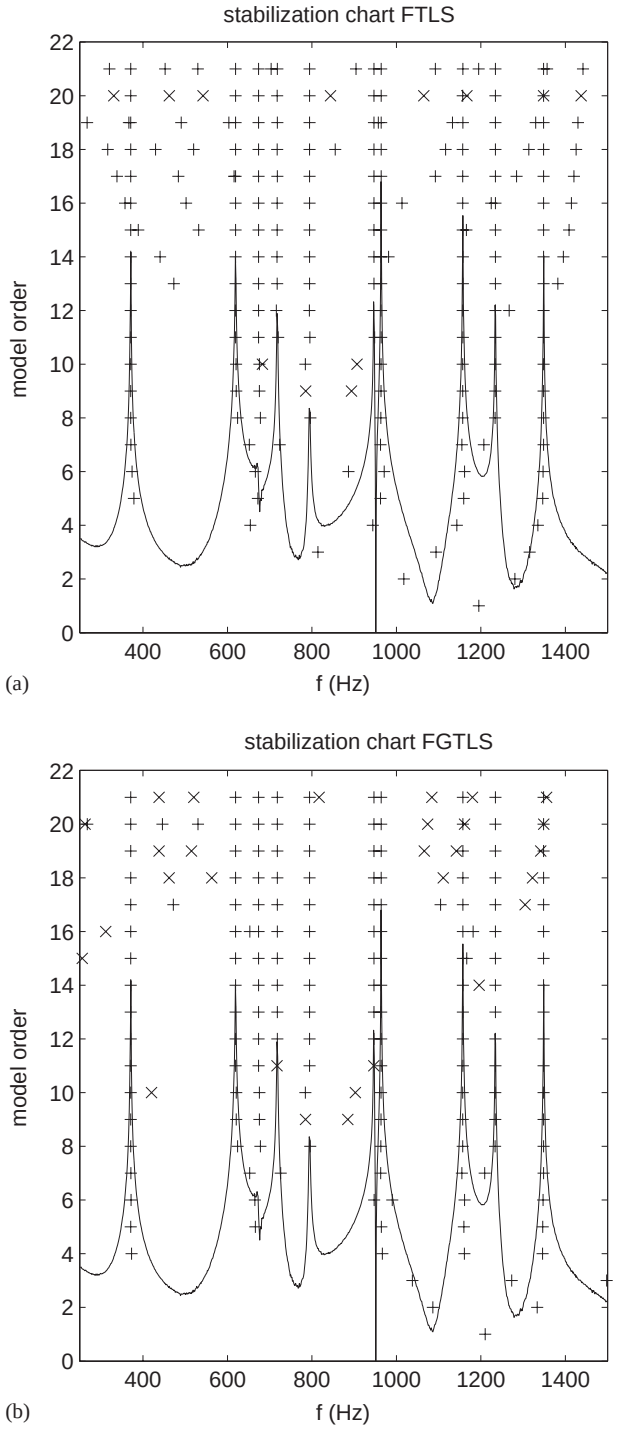

Fig. 6. Stabilization chart with the stable (+) and unstable (×) poles using FTLS (a), FGTLS (b).

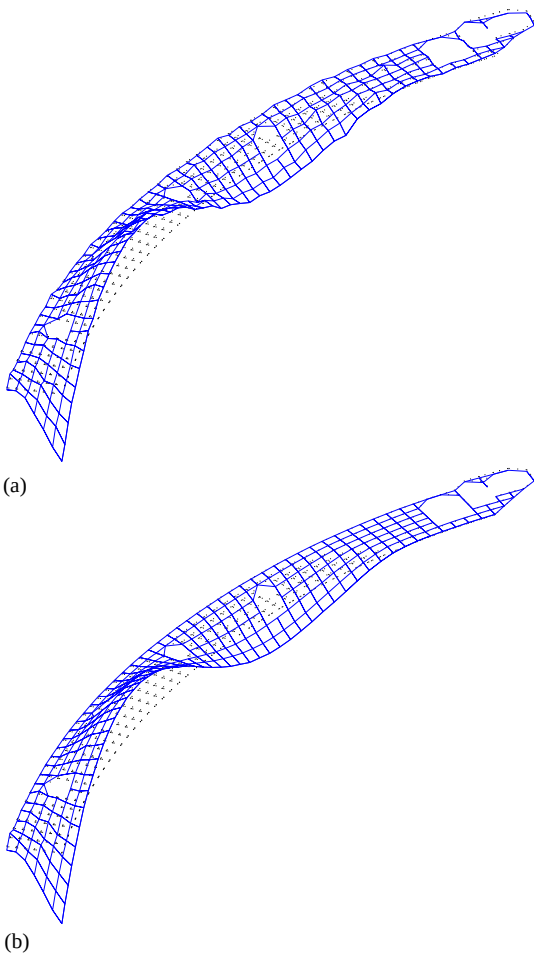

Fig. 7. Slat track mode shape for the mode at 1234Hz using FTLS (a), FGTLS (b).

$N_i = 1$) and model order n (with $N_o = 10$, $N_i = 1$). Considering the output dimension N_o, the results indicate that the GTLS problem is solved in $\mathcal{O}(N_o^3)$ flops, whereas $\mathcal{O}(N_o)$ flops for the FGTLS, resulting in a gain of $\mathcal{O}(N_o)^2$ flops, explained by the elimination approach. On the other hand, for an increasing model order, the number of flops used by the GTLS and FGTLS is similar, i.e., $\mathcal{O}(n^3)$.

6. Conclusions

A fast implementation of the frequency-domain input–output GTLS estimator makes it suitable to analyze large amounts of modal data within an Errors-in-Variables framework. This algorithm is preferable to classical FRF-based curve-fitting methods, certainly in the case when periodic excitation is applied and hence an errors-in-variables noise model can be determined. The proposed GTLS algorithm provides accurate modal parameter estimation by the integration of

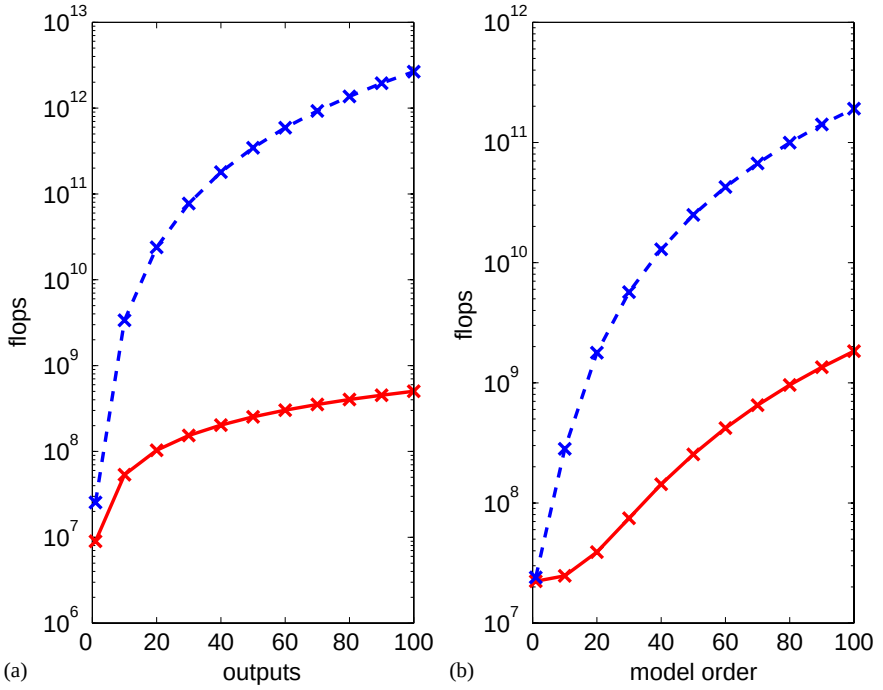

Fig. 8. Flops count for GTLS (dashed line) and FGTLS (solid line) for varying number of (a) outputs and (b) model order.

this noise model in the parametric identification process. Although a linear approximation is necessary to obtain a fast GTLS implementation, Monte Carlo simulations show that only a very small loss of accuracy appears for very high noise levels on the inputs. As a result, in practice the fast GTLS algorithm has very similar statistical properties as the exact GTLS. Both accuracy as well as computation speed and memory usage are important issues for modal analysis applications, such as for modal-based design and comfort improvement, damage assessment and structural health monitoring, and finite element model updating.

Acknowledgements

The financial support of the Institute for the Promotion of Innovation by Science and Technology in Flanders (IWT), the Concerted Research Action "OPTIMech" of the Flemish Community and the Research Council (OZR) of the Vrije Universiteit Brussel (VUB) are gratefully acknowledged.

References

[1] S. Van Huffel (Ed.), *Recent Advances in Total Least Squares Techniques and Errors-in-Variables Modeling*, SIAM, Philadelphia, PA, 1997.

[2] R. Pintelon, P. Guillaume, G. Vandersteen, Y. Rolain, Analysis, development and application of TLS algorithms in frequency domain system identification, *SIAM Journal on Matrix Analyses and Applications* 19 (4) (1998) 983–1004.
[3] N.M.M. Maia, J.M.M. Silva (Eds.), *Theoretical and Experimental Modal Analysis*, Research Studies Press, Somerset, 1997.
[4] J.J. Juang, *Applied System Identification*, Prentice-Hall, Englewood Cliffs, NJ, 1994.
[5] M.H. Richardson, D.L. Formenti, Global curve fitting of frequency response measurements using the rational fraction polynomial method, in: *Proceedings of the Third International Modal Analysis Conference*, Orlando, FL, 1985, pp. 390–397.
[6] H. Van der Auweraer, J. Leuridan, Multiple input orthogonal polynomial parameter estimation, *Mechanical Systems and Signal Processing* 1 (3) (1987) 259–272.
[7] P. Verboven, *Frequency-domain System Identification for Modal Analysis*, Ph.D. Thesis, Vakgroep WERK, VUB, Brussels, Belgium, May 2002.
[8] P. Guillaume, Frequency response measurements of multivariable systems using nonlinear averaging techniques, *IEEE Transactions on Instrumentation and Measurement* 47 (3) (1998) 796–800.
[9] P. Verboven, M. Van Overmeire, P. Guillaume, S. Vanlanduit, Improved frequency-domain total least squares identification for modal analysis applications, in: *Proceedings of the Fifth National Congress on Theoretical and Applied Mechanics*, Louvain-la-Neuve, Belgium, 2000, pp. 211–214.
[10] T. Kailath, *Linear Systems*, Prentice-Hall, Englewood Cliffs, NJ, 1980.
[11] J. Schoukens, R. Pintelon, G. Vandersteen, P. Guillaume, Frequency-domain system identification using non-parametric noise models estimated from a small number of data sets, *Automatica* 33 (6) (1997) 1073–1086.
[12] R. Pintelon, J. Schoukens, G. Vandersteen, Frequency-domain system identification using arbitrary signals, *IEEE Transactions on Automatic Control* 42 (12) (1997) 1717–1720.
[13] P. Verboven, P. Guillaume, B. Cauberghe, S. Vanlanduit, E. Parloo, Modal parameter estimation from input–output Fourier data using frequency-domain maximum likelihood identification, *Journal of Sound and Vibration*, 2004, in press.
[14] J. Schoukens, Y. Rolain, F. Gustaffson, R. Pintelon, Fast calculation of least-squares estimates for system identification, in: *Proceedings of the 32nd Decision and Control Conference*, Tampa, FL, 1998, pp. 3408–3410.
[15] P. Guillaume, P. Verboven, S. Vanlanduit, Frequency-domain maximum likelihood identification of modal parameters with confidence intervals, in: *Proceedings of the 23rd International Seminar on Modal Analysis*, Leuven, Belgium, 1998, pp. 359–366.
[16] Y. Rolain, R. Pintelon, K.Q. Xu, H. Vold, Best conditioned parametric identification of transfer function models in the frequency domain, *IEEE Transactions an Automatic Control* 40 (11) (1995) 1954–1960.
[17] H. Van der Auweraer, P. Guillaume, P. Verboven, S. Vanlanduit, Application of a fast-stabilizing frequency domain parameter estimation method, *American Societ of Mechanical Engineers, Journal of Dynamic Systems, Measurement and Control* 123 (4) (2001) 651–658.
[18] S. Van Huffel, J. Vandewalle, *The Total Least Squares Problem: Computational Aspects and Analysis*, SIAM, Philadelphia, PA, 1991.